The Small-Scale Mixing of Clouds with their Environment: Impacts on Micro- and Macroscale Cloud Properties

F. Hoffmann

Meteorologisches Institut, Ludwig-Maximilians-Universität München, Munich, Germany

Corresponding author: Fabian Hoffmann, fa.hoffmann@physik.uni-muenchen.de

Abstract

The small-scale mixing of clouds with their environment is an essential cloud process. Following an entrainment event, turbulent mixing breaks down the entrained air and homogenizes it with the cloud, covering multiple orders of magnitude in lengthscales from the entraining eddies ($\sim$ 100 m) down to the Kolmogorov length ($\sim$ 1 mm). The character of this process, traditionally categorized into homogeneous and inhomogeneous mixing scenarios, can affect the microphysical composition of clouds, with commensurate impacts on large-scale cloud properties such as the cloud albedo and cloud lifetime.

Based on the current physical understanding of the small-scale mixing of cloudy and cloud-free air, this chapter will summarize the basic theories describing this process. By considering the wide range of involved scales, we will outline different observational and numerical approaches used to investigate this process in clouds, as well as methods to parameterize it in large-scale numerical models. Finally, we will review the impacts of the small-scale mixing process, focusing on microscale changes in the droplet size distribution as well as macroscale effects relevant to our understanding of clouds in the climate system.

1 Introduction

One major role of clouds in the climate system stems from their ability to reflect incident shortwave radiation back to space, resulting in a major negative forcing on the global radiation budget [e.g., *Boucher et al.*, 2013]. This forcing, often quantified as the cloud radiative effect [*Betts*, 2007], is proportional to the product of cloud albedo and cloud fraction, where the former is primarily determined by the cloud microphysical composition — the number and size of droplets forming the droplet size distribution — and the latter is controlled by the cloud macroscale — the large-scale organization of clouds and their lifecycle.

Historically, the influence of cloud microphysics on the cloud radiative effect were attributed to two processes: The *albedo effect* predicts that a higher droplet concentration results in a higher cloud albedo due to the larger integral droplet surface capable of reflecting more shortwave radiation [*Twomey*, 1974, 1977]. The *lifetime effect* indicates that a higher droplet number concentration with commensurately smaller droplets may prevent droplets from colliding, and hence decelerates the decay of clouds by precipitation, increasing cloud lifetime and cloud fraction [*Albrecht*, 1989]. In more recent years, our understanding of these effects and their implications for the global climate has been significantly widened by amending the underlying physical framework by the turbulent nature of clouds [e.g., *Bodenschatz et al.*, 2010], including, inter alia, the entrainment of cloud-free air and its subsequent mixing with the cloud, which is the main topic of this chapter.

The mixing of cloudy and cloud-free air can have important implications for the role of clouds in the climate system, bounded by the canonical scenarios of *homogeneous* and *extreme inhomogeneous mixing* [*Warner*, 1973; *Baker and Latham*, 1979]. While these terms and their distinct effects on the micro- and macroscale properties of clouds will be defined more carefully in the following, it is important to note that the assumption of one mixing scenario over the other can be of great consequence. For instance, extreme inhomogeneous instead of homogeneous mixing is able to reduce the albedo of a cloud by up to 6 percentage points [*Chosson et al.*, 2007; *Slawinska et al.*, 2008]. Furthermore, inhomogeneous mixing might also accelerate the growth of cloud droplets, which can imperil the colloidal stability of clouds by initiating the precipitation process, with commensurate negative effects on cloud lifetime and cover [e.g., *Baker et al.*, 1980].

While turbulence is the main driver for these effects, it has further effects on clouds that are not covered in this chapter. Therefore, the interested reader is referred to *Shaw* [2003], *Devenish et al.* [2012], and *Grabowski and Wang* [2013] for more information on turbulence-induced supersaturation fluctuations, droplet clustering, including related particle inertia ef-

fects, as well as turbulence-enhanced collision rates. Furthermore, this chapter can be seen as an addendum to *de Rooy et al.* [2013], who reviewed the entrainment process from a large-scale perspective, but did not address the small-scale detail of the subsequent mixing process presented here. Finally, it is necessary to state that this chapter is limited to shallow clouds, free from frozen hydrometeors. While the turbulent mixing of cloudy with cloud-free air is also relevant for mixed-phase and cold clouds, the literature on this topic is still very limited and therefore omitted [e.g., *Korolev et al.*, 2017; *Hoffmann*, 2020].

The chapter is organized as follows. First, we will summarize the basic processes of entrainment and small-scale mixing in warm clouds (Sec. 2). Then, the theoretical framework to describe the small-scale mixing process in clouds is introduced (Sec. 3), followed by an overview of observational techniques and numerical models used to investigate it (Sec. 4). Based on this, we will explore the effects of small-scale mixing on micro- and macroscale cloud properties (Sec. 5), before this chapter is concluded (Sec. 6).

2 Entrainment and Mixing in Warm Clouds

Beginning with *Stommel* [1947] and *Warner* [1955], the entrainment of cloud-free air into clouds has been recognized as an essential process to understand the observed liquid water content of clouds, which is lower than the expected adiabatic values due to the mixing with cloud-free air. Today, we generally understand that the cloud-free air is entrained into the cloud by the specific large-scale dynamics of the cloud, i.e., the vortical motion of the ascending cumulus cloud top which engulfs cloud-free air laterally [*Grabowski and Clark*, 1993; *Zhao and Austin*, 2005; *Heus et al.*, 2008], or the downward branches of the stratocumulus-topped boundary layer large-eddy circulation which engulf air from above the cloud top [*Nicholls*, 1989; *Gerber et al.*, 2005; *Kurowski et al.*, 2009; *Yamaguchi and Randall*, 2012]. These entraining motions create regions of negligible liquid water inside the cloud, so-called *cloud holes*, which are continuously deformed [e.g., *Krueger*, 1993]. This marks the beginning of the actual mixing process. Initially, this process is driven by the entraining eddy, and later by the developing small-scale turbulence that folds and stretches the cloud hole into increasingly smaller filaments until the Kolmogorov lengthscale is reached. At this lengthscale, molecular diffusion homogenizes the entrained air with the cloud. Throughout this turbulent break-down process, the increasing surface area of the cloud hole exposes more and more droplets to a subsaturated environment where they evaporate. Accordingly, the mixing process combines the turbulent stirring of cloudy and cloud-free air with the commensurate droplet evaporation.

Traditionally, the mixing process in clouds has gained less attention than the entrainment. In fact, mixing is often implicitly included in the broader term entrainment, although only the mixing process causes the evaporation that results in the sub-adiabatic liquid water content initially observed by *Stommel* [1947] and *Warner* [1955]. Nonetheless, *Warner* [1969a] hypothesized that mixing is relevant for the development of the broad droplet size distributions typically observed in clouds, but was not able to explain the size distributions theoretically. The reason for this was the common depiction of mixing as an instantaneous process, i.e., cloud-free and cloudy air homogenize rapidly after entrainment, which causes all droplets to experience the same subsaturation and to evaporate similarly, with only minuscule effects on the droplet size distribution [*Warner*, 1973].

Later, this depiction of the mixing process has been challenged by *Latham and Reed* [1977] and *Baker and Latham* [1979], who began to consider that the mixing process is not instantaneous. A finite rate mixing process allows some droplets to be located within unblemished cloudy filaments, while only those droplets at the cloudy filament edges evaporate if they leave the cloud. Since this process allows for a nonidentical development of droplet sizes, a broad droplet size distributions can be produced which is much more in agreement with those observed in clouds [e.g., *Warner*, 1969a].

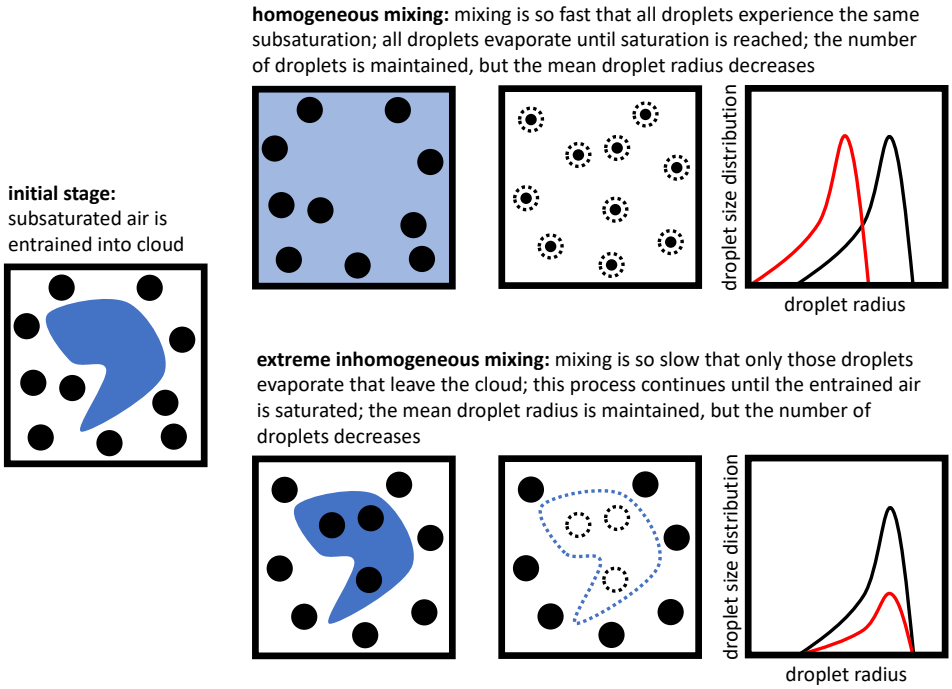

Figure 1. This figure illustrates the two limiting scenarios of homogeneous and extreme inhomogeneous mixing following an idealized entrainment event. The entrained air is depicted in shades of blue, indicating the subsaturated cloud-free air. Black dots represent cloud droplets. The rightmost panels show the reaction of the droplet size distribution on the respective mixing scenarios, where the black (red) line indicates the droplet size distribution before (after) mixing.

Both processes can be idealized as *homogeneous* and *extreme inhomogeneous mixing*, respectively, which are illustrated in Fig. 1. During *homogeneous mixing*, which typically occurs under rapid turbulent mixing, all droplets evaporate, but none completely. Accordingly, homogeneous mixing is often identified by a constant droplet number concentration. If, however, the turbulent mixing is comparatively slow, only those droplets evaporate that leave the cloudy filaments. If the droplets that leave the cloud evaporate completely, the mean droplet radius is maintained and the scenario is called *extreme inhomogeneous mixing*. Homogeneous and extreme inhomogeneous mixing limit the range of mixing scenarios that occur in nature. Intermediate mixing scenarios, in which both the mean droplet radius and droplet number change, are generally termed inhomogeneous mixing, and it can be necessary to distinguish them from the case of extreme inhomogeneous mixing.

Finally, it is important to note that real clouds constitute a much more complicated system than this idealized depiction of the mixing process can cover. Real clouds experience several, potentially interacting entrainment events on multiple scales, making it probably impossible to ever reach a final state in which all heterogeneities caused by entrained are homogenized [e.g., *Cooper*, 1989]. Nonetheless, the theoretical framework that builds upon the definitions of homogeneous and extreme inhomogeneous mixing is a starting point to understand the effects of small-scale mixing in clouds, which will be continued in the next section.

3 The Theory of Small-Scale Mixing

The last section indicated that small-scale mixing can be understood from two viewpoints, which are either the speed with which the turbulent mixing progresses or the effect of

the mixing on the cloud microphysical composition, i.e., the droplet number and size. In this section, we will introduce two theoretical frameworks that are based on these viewpoint: the Damköhler number (Sec. 3.1) and the microphysical mixing diagram (Sec. 3.2).

3.1 The Damköhler Number

When does a homogeneous or inhomogeneous mixing scenario occur? While the actual mixing scenario is usually determined by the changes in droplet number and size, comparing the respective timescales for the turbulent mixing to the microphysical reaction timescale, i.e., the evaporation of droplets, can indicate which mixing scenario is favored. The ratio of these timescales, which will be defined in detail below, is termed the Damköhler number

$$\mathrm{Da} = \frac{\tau_{\mathrm{mixing}}}{\tau_{\mathrm{micro}}}, \tag{1}$$

which has been originally proposed in the turbulent combustion literature [e.g., *Peters*, 2000], and has been adapted to understand the effects of turbulence on cloud microphysics subsequently [e.g., *Baker et al.*, 1980; *Shaw*, 2003]. If $\mathrm{Da} \gg 1$, the turbulent mixing is much slower than the microphysical reaction ($\tau_{\mathrm{mixing}} \gg \tau_{\mathrm{micro}}$). Accordingly, an inhomogeneous mixing scenario is favored since only those droplets evaporate that leave the cloudy filaments. If $\mathrm{Da} \ll 1$, the turbulent mixing is much faster than the microphysical reaction ($\tau_{\mathrm{mixing}} \ll \tau_{\mathrm{micro}}$), and differences between cloudy and cloud-free air vanish rapidly. Thus, a homogeneous mixing scenario is likely since all droplets experience a similar subsaturation and therefore react similarly. Note, however, that distinct filaments of cloudy and cloud-free air may exist on scales as small as the Kolmogorov scale, even in the homogeneous limit of the Damköhler number. However, the microphysical reaction is so slow that these small-scale differences in supersaturation do not affect the evaporation of droplets.

Two timescales are traditionally considered to determine τ_{micro}. First, we can calculate the time a droplet of radius r requires to evaporate completely [e.g., *Baker et al.*, 1980]:

$$\tau_{\mathrm{evap}} = r^2 \frac{F_{\mathrm{k}} + F_{\mathrm{D}}}{2|S|}, \tag{2}$$

where $S < 0$ is the subsaturation to which the droplets are exposed, and $F_{\mathrm{k}} + F_{\mathrm{D}}$ are parameters depending on heat conduction and molecular diffusion of water vapor, respectively. A second microphysical timescale can be obtained by the time necessary to saturate subsaturated air by the evaporation of droplets [*Squires*, 1952]. The e-folding timescale for this process is called the phase relaxation timescale, and is calculated as

$$\tau_{\mathrm{phase}} = (4\pi D_{\mathrm{v}} r_{\mathrm{m}} N)^{-1}, \tag{3}$$

where r_{m} is the arithmetic mean droplet radius and N the droplet number concentration. D_{v} is an effective water vapor diffusion coefficient, which is based on the molecular vapor diffusion coefficient but modified to account for the additional cooling (heating) of droplets during evaporation (condensation), which slows down vapor diffusion (see Eqns. (11) and (14) in *Kumar et al.* [2013]).

Note, however, there is no consensus on which microphysical timescale is preferable for understanding small-scale mixing in clouds. *Feingold and Siebert* [2009] argue that under typical conditions, both timescales exhibit similar values between 1 and 10 s. Choosing the minimum of τ_{evap} and τ_{phase}, however, may avoid infinite values occurring in almost saturated conditions or for clouds with vanishing droplet sizes. *Lehmann et al.* [2009] and *Lu et al.* [2018] show that τ_{evap} is more appropriate for studies on changes in the droplet size distributions, while τ_{phase} should be applied if changes in the liquid water content are of interest. Furthermore, τ_{micro} can be extended to other microphysical processes than (2) and (3). The activation of droplets occurs on timescales significantly smaller than one second [*Hoffmann et al.*, 2017; *Arabas and Shima*, 2017], and is therefore highly susceptible to turbulent mixing processes as also indicated by *Abade et al.* [2018].

The time to entirely mix the entrained air with the cloud is approximated by the time required to break a blob of entrained air down to the Kolmogorov lengthscale. Below this lengthscale, viscous forces dominate, which naturally terminate turbulent mixing and molecular diffusion concludes homogenization. This so-called *mixing timescale* can be obtained from inertial range scaling as

$$\tau_{\text{mixing}} = \left(\frac{l^2}{\epsilon}\right)^{1/3}, \tag{4}$$

where ϵ is the turbulent energy dissipation rate, which is a measure of the turbulence intensity, and l is the characteristic lengthscale of the blob of entrained air [e.g., *Baker et al.*, 1984].

With these definitions, the Damköhler number does not only allow to determine when a mixing process is likely to be homogeneous (Da $\ll$ 1) or inhomogeneous (Da $\gg$ 1), it also allows to determine the scale at which the mixing transitions from inhomogeneous to homogeneous mixing. Following *Baker et al.* [1980] and *Lehmann et al.* [2009], this is done by setting Da = 1 and solving Eqn. (1) for l. The resulting *transition lengthscale* is

$$l_{\text{trans}} = \epsilon^{1/2}\tau_{\text{micro}}^{3/2}, \tag{5}$$

which separates the lengthscales at which spatial differences in the thermodynamic conditions matter and mixing is likely to be inhomogeneous ($l \gg l_{\text{trans}}$) from the lengthscales at which small-scale mixing is rapid, and a homogeneous mixing scenario is favored ($l \ll l_{\text{trans}}$). Accordingly, for typical values of τ_{micro} (2 s) and ϵ (10^{-3} m^2 s^{-3} for stratocumulus and 10^{-2} to 10^{-1} m^2 s^{-3} for cumulus), the transition from inhomogeneous to homogeneous mixing occurs on a lengthscale between 10 to 100 cm [e.g., *Lehmann et al.*, 2009], which is smaller than the resolution of most numerical models used to simulate clouds. Since most models treat unresolved mixing processes as homogenous by design, the transition lengthscale also defines the minimum resolution that would be required to represent inhomogeneous small-scale mixing and its effects on cloud microphysics successfully. However, resolving l_{trans} imposes significant computational constraints, which limit the application of numerical cloud models to study small-scale mixing processes, as discussed further in Sec. 4.

Finally, a refinement on the mixing timescale and the transition lengthscale needs to be made. Turbulence is not the only process that changes the thermodynamical conditions experienced by a droplet. Once a droplet is large enough to sediment significantly, it may fall from a saturated volume of air into a subsaturated, smearing out the boundary conditions for the microphysical reaction [e.g., *Jensen and Baker*, 1989; *Grabowski*, 1993; *Tölle and Krueger*, 2014]. The characteristic timescale for this is termed the sedimentation timescale, and can be obtained as

$$\tau_{\text{sedi}} = \frac{l}{w_{\text{sedi}}}, \tag{6}$$

where w_{sedi} is the droplet sedimentation velocity and l the aforementioned characteristic lengthscale of the entrained air. The inverse sum of τ_{mix} and τ_{sedi} yields an effective mixing timescale

$$\tau^*_{\text{mix}} = (\tau^{-1}_{\text{mix}} + \tau^{-1}_{\text{sedi}})^{-1}, \tag{7}$$

which should be used instead of τ_{mix}. Using τ^*_{mix} makes the analytical derivation of an effective transition lengthscale cumbersome. However, by neglecting non-linear dependencies on w_{sedi}, the effective transition lengthscale can be approximated as

$$l^*_{\text{trans}} \approx \epsilon^{1/2}\tau_{\text{micro}}^{3/2} + w_{\text{sedi}}\tau_{\text{micro}}, \tag{8}$$

which indicates that droplets starting to be relevant for collision and coalescence ($r > 20\,\mu$m, $w_{\text{sedi}} > 5$ cm s^{-1}) may double the transition lengthscale, with commensurate stronger effects for even larger droplets. Accordingly, inhomogeneous mixing and its effects become increasingly irrelevant for larger droplets [e.g., *Grabowski and Vaillancourt*, 1999].

3.2 The Mixing Diagram

The Damköhler number and the equivalent transition lengthscale help to understand where to expect inhomogeneous or homogeneous mixing processes. However, they cannot be used to infer a specific mixing scenario. For that, a functional relationship between the droplet size and droplet number is needed, and it is usually presented in the form of a microphysical *mixing diagram* [*Burnet and Brenguier*, 2007]. A typical mixing diagram is depicted in Fig. 2.

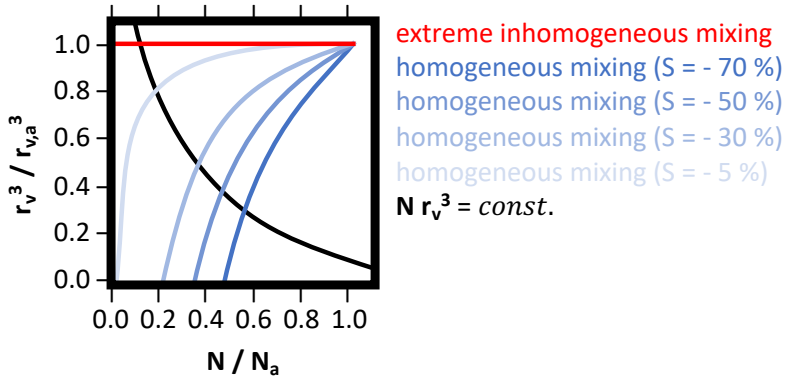

Figure 2. This idealized mixing diagram illustrates how the normalized mean volume radius $r_\mathrm{v}^3/r_\mathrm{v,a}^3$ depends on the normalized droplet number concentration N/N_a for extreme inhomogeneous mixing (red line) and homogeneous mixing (blue lines) for different saturation ratios of the entrained air (shades of blue). The black line indicates $Nr_\mathrm{v}^3 = const.$, and accordingly all intermediate mixing scenarios between homogeneous and extreme inhomogeneous mixing. Mixing diagrams of this type have been introduced by *Burnet and Brenguier* [2007].

The mixing diagram shows how the (cubed) mean volume radius r_v^3 changes as a function of the droplet number concentration N under a prescribed mixing scenario. The cubed mean volume radius can be calculated from the liquid water content $q_\mathrm{l} = 4/3\pi\rho_\mathrm{l} r_\mathrm{v}^3 N$ once N is known, making it easily available from measurements. ρ_l is the mass density of water. Note that r_v^3 and N represent the microphysical state after the entrainment and mixing process is finished, and are normalized by their respective values before entrainment and mixing, $r_\mathrm{v,a}^3$ and N_a. $r_\mathrm{v,a}^3$ and N_a are typically unknown in less idealized (i.e., realistic) applications. Therefore, adiabatic values are often used as a proxy.

Changes in $r_\mathrm{v}^3/r_\mathrm{v,a}^3$ for the homogeneous and extreme inhomogeneous limit can be determined from the q_l which is obtained once entrainment and the subsequent mixing are finished. Since the amount of liquid water that needs to be evaporated to saturate the mixture of subsaturated entrained and saturated cloudy air does not depend on the mixing scenario, q_l can be generally expressed as

$$q_\mathrm{l} = (1-\mu)q_\mathrm{l,a} + \mu\delta q. \tag{9}$$

Here, the first term on the right-hand side represents the dilution of the considered volume of air by entrainment, where μ is the mass fraction of the entrained air. The second term represents the necessary evaporation to saturate the mixed air, where $\delta q = S/A \leq 0$ is the saturation deficit of the entrained air, which is determined by its saturation ratio S and a parameter A, which is a function of temperature and pressure. (The reader is referred to *Korolev et al.* [2016] for a detailed derivation of Eqns. (9) through (14).)

The droplet number concentration after entrainment, but before mixing, can be derived analogously. Since the entrained air is assumed to contain no droplets, the corresponding

droplet number concentration decreases as

$$N_\mathrm{h} = N_\mathrm{a}(1-\mu), \tag{10}$$

which is also the droplet number concentration after homogeneous mixing, during which droplets are assumed to not evaporate completely. By introducing (10) into (9), we determine

$$\frac{r_\mathrm{v,h}^3}{r_\mathrm{v,a}^3} = 1 + \frac{1 - N_\mathrm{h}/N_\mathrm{a}}{N_\mathrm{h}/N_\mathrm{a}} \frac{\delta q}{q_\mathrm{l,a}}, \tag{11}$$

which describes the reduction in mean volume radius under homogeneous mixing as shown in Fig. 2 (blue lines). Note that the decrease of $r_\mathrm{v,h}^3/r_\mathrm{v,a}^3$ is stronger for drier entrained air. In fact, if the entrained air is very dry (or the fraction of entrained air is sufficiently large), it might not possible to saturate the mixture and a mixing diagram cannot be derived. On the other hand, very humid entrained air requires only minuscule evaporation, making homogeneous and extreme inhomogeneous mixing (red line) almost indistinguishable based on their microphysical reaction. Accordingly, this scenario might be considered a *degenerate* mixing case, in which homogeneous and extreme inhomogeneous mixing result in the same microphysical reaction [*Korolev et al.*, 2016; *Pinsky et al.*, 2016].

During extreme inhomogeneous mixing, the mean volume radius does not change, which results in the constant relationship

$$\frac{r_\mathrm{v,i}^3}{r_\mathrm{v,a}^3} = 1, \tag{12}$$

shown in Fig. 2 (red line). Inserting (12) in (9), the droplet number concentration under extreme inhomogeneous mixing can be determined as

$$\frac{N_\mathrm{i}}{N_\mathrm{a}} = \frac{q_\mathrm{l}}{q_\mathrm{l,a}}, \tag{13}$$

or, equivalently, as

$$N_\mathrm{i} = (1-\mu)N_\mathrm{a} + \frac{\mu \delta q}{\frac{4}{3}\pi \rho_\mathrm{l} r_\mathrm{v,a}^3}, \tag{14}$$

where the first term on the right-hand side represents the dilution due to entrainment (analogous to homogeneous mixing shown in Eqn. (10)), and the second term is the decrease in droplet number concentration due to extreme inhomogeneous mixing, i.e., the fraction of droplets that evaporates completely to saturate the entrained air.

But how does microphysics respond to a mixing scenario between extreme inhomogeneous and homogeneous mixing in which both mean volume radius and droplet number concentration change? Since the liquid water content after mixing is independent of the mixing scenario unless all droplets evaporate completely, see Eq. (9), all possible mixing scenarios obey

$$r_\mathrm{v}^3 N = r_\mathrm{v,h}^3 N_\mathrm{h} = r_\mathrm{v,i}^3 N_\mathrm{i} = const., \tag{15}$$

which is marked by the black line in Fig. 2. This expression can be generalized as

$$\frac{N}{N_\mathrm{h}} = \left(\frac{r_\mathrm{v,h}^3}{r_\mathrm{v,i}^3} \right)^\alpha, \tag{16}$$

which results in homogeneous mixing for $\alpha = 0$, and in extreme inhomogeneous mixing for $\alpha = 1$. Intermediate values of $0 \leq \alpha \leq 1$ are expected for varying degrees of inhomogeneous mixing. Accordingly,

$$\alpha = \frac{\ln(N/N_\mathrm{h})}{\ln(r_\mathrm{v,h}^3/r_\mathrm{v,i}^3)} \tag{17}$$

can be used as a simple metric to characterize observed or simulated mixing scenarios [*Morrison and Grabowski*, 2008; *Andrejczuk et al.*, 2009; *Lu et al.*, 2013]. Furthermore, α can be used to parameterize inhomogeneous mixing in numerical models as explained further in Sec. 4.2.3.

Finally, note that even under conditions that favor homogeneous mixing (Da $\ll$ 1), N is not necessarily conserved. If the droplet size distribution exhibits sufficiently small droplets, some of them will evaporate completely, irrespective of the mixing scenario, resulting in an apparently inhomogeneous mixing scenario [*Tölle and Krueger*, 2014; *Luo et al.*, 2020]. Similarly, entrained air might contain aerosol particles that activate to the droplets during the mixing process, which can increase N [e.g., *Slawinska et al.*, 2012]. Accordingly, an inhomogeneous mixing scenario can appear more homogeneous than expected (Da $\gg$ 1).

4 Investigating Small-Scale Mixing

In this section, we will present approaches to investigate small-scale mixing in observations and numerical modeling. All these approaches have to cope with the multiscale nature of clouds, ranging from entire cloud fields ($\sim$ 100 km) to the smallest scales of turbulent mixing ($\sim$ 1 mm), and cloud microphysics ($\sim$ 10 μm). No approach is able to cover all these scales, and neglecting or idealizing smaller or larger scales is inherent to all methods.

4.1 Observations

Observations are the cornerstone of physics, and airborne measurements enabled important insights on entrainment and mixing in clouds [e.g., *Warner*, 1969a; *Jensen et al.*, 1985; *Paluch and Knight*, 1984; *Blyth et al.*, 1988; *Gerber et al.*, 2008]. Observing the effects of small-scale mixing on clouds is, at first glance, relatively simple, since simultaneous measurements of the droplet number concentration and droplet radii are available for at least 50 years.

However, early instruments, such as sooted glass slides used to collect droplets outside the airplane, exhibited very slow sampling rates on the order of 1 Hz [*Warner*, 1969a]. Due to the comparably high airspeed of planes ($\sim$ 100 m s^{-1}), many airborne measurements of the past did therefore not resolve scales below 100 m, which made it impossible to detect variations on scales as small as the transition lengthscale directly. Thus, by erroneously assuming that the measured droplet concentrations and droplet sizes are spatially uniform, it has been believed that clouds might mix homogeneously. However, the simultaneous presence of small-scale filaments of cloudy and cloud-free air, in agreement with our current depiction of inhomogeneous mixing, can result in the same measurements when averaged over the aforementioned lengthscale imposed by insufficient sampling rates, as first discussed by *Paluch* [1986] and *Paluch and Baumgardner* [1989]. Today, measurements are commonly provided by instruments such as the Forward Scattering Spectrometer Probe (FSSP) [*Brenguier*, 1993; *Brenguier et al.*, 1998] or the Particle Volume Monitor (PVM) [*Gerber et al.*, 1993] with sampling rates on the order of 1000 Hz, which enables direct observations of small-scale mixing from airplanes.

A further improvement can be achieved by lowering the airspeed, which can be done by using helicopters instead of airplanes. The Airborne Cloud Turbulence Observation System (ACTOS) [*Siebert et al.*, 2006], for instance, can be suspended from helicopters, providing sufficiently resolved measurements to detect even the finest scales of turbulent processes in clouds [e.g., *Siebert et al.*, 2013]. Furthermore, the increasing use of holographic systems, such as the Holographic Detector for Clouds (HOLODEC), allow three-dimensional snapshots of the small-scale distribution of cloud droplets, including sharp gradients between cloudy and non-cloudy filaments as they are expected to be observed during inhomogeneous mixing [*Beals et al.*, 2015]. While holographic systems can provide a glimpse into the three-dimensional small-scale distribution of droplets, their sample volume ($\sim$ 15 cm^3) is too lim-

ited to capture all relevant scales of the mixing process. Entire clouds, may be sampled in the near future using several remotely piloted aircrafts (RPAs, commonly known as drones), as proposed in a current assessment study [*Maury et al.*, 2021].

Finally, laboratory cloud chamber measurements, as they are currently undertaken in the Π-chamber or similar facilities [e.g., *Chang et al.*, 2016], may also enable deeper observational process-level understanding of entrainment and mixing once appropriate scales can be accommodated [*Shaw et al.*, 2020].

4.2 Numerical Modeling

Turbulent mixing processes are ubiquitous, and have been extensively investigated in engineering applications such as turbulent combustion [e.g., *Peters*, 2000]. Therefore, many of the following numerical models originate from the engineering literature, and have been adapted to explore cloud physics questions. However, to accommodate the large range of relevant scales, multiple modeling approaches are necessary to cover all aspects of the mixing process. Accordingly, we will present models for representing cloud microphysics first (Sec. 4.2.1). Then, fluid dynamics models for the investigation of small-scale mixing at the Kolmogorov lengthscale are presented (Sec. 4.2.2). Due to the limited computational resources, these models are restricted toward larger scales. Models which represent these larger scales are not able to resolve small-scale mixing explicitly, and parameterizations are applied to represent potentially inhomogeneous mixing scenarios, which are summarized is the last subsection (Sec. 4.2.3).

4.2.1 Cloud Microphysical Models

Cloud microphysical models predict parameters describing the microphysical state of a cloud, applying varying degrees of complexity. The reader is referred to *Morrison et al.* [2020] for a recent review of cloud microphysical modeling approaches.

To a certain degree, all commonly applied cloud microphysical models are able to represent the effects of small-scale mixing on the cloud microphysical composition. Without restrictions, this is possible in detailed models that predict the entire droplet size distribution by solving equations that describe the condensation and evaporation of droplets, their activation from aerosols, as well as collision processes. Thus, changes in the droplets size distribution due to small-scale mixing can be considered directly. Traditionally, these detailed models have been *bin* or *spectral models*, which represent the droplet size distribution on a numerical grid in radius space [e.g., *Tzivion et al.*, 1987; *Bott*, 1998]. Today, an increasing number of similarly detailed *Lagrangian cloud models* is applied, which represent the droplet size distribution by several individually simulated computational particles, each representing just one droplet or a multitude of identical droplets (so-called superdroplets) [e.g., *Andrejczuk et al.*, 2008; *Shima et al.*, 2009; *Hoffmann et al.*, 2015]. *Bulk models*, however, represent the droplet size distribution by idealized functions, and predict one or several statistical moments of it. To represent the basic impacts of small-scale mixing, bulk models are required to predict at least two moments, N and q_l [e.g., *Khairoutdinov and Kogan*, 2000; *Milbrandt and Yau*, 2005; *Morrison et al.*, 2005; *Seifert and Beheng*, 2006; *Thompson and Eidhammer*, 2014]. Additional moments are necessary to represent the impact of small-scale mixing on the width of the droplet size distribution, as discussed in Sec. 5.1.

4.2.2 Direct Modeling of Turbulent Mixing

The most direct approach to simulate small-scale mixing is to employ *direct numerical simulations* (DNSs) that solve the three-dimensional Navier-Stokes equations applying a resolution that matches the Kolmogorov lengthscale [e.g., *Moin and Mahesh*, 1998]. Due to computational constraints, the model domain is restricted to a cube with a typical edge length of a couple of decimeters, even on today's supercomputers [*Vaillancourt et al.*, 2001,

2002; *Andrejczuk et al.*, 2009; *Kumar et al.*, 2013; *Perrin and Jonker*, 2015; *Götzfried et al.*, 2017; *Kunishima and Onishi*, 2018; *Gao et al.*, 2018]. Accordingly, these models simulate small-scale mixing close to the typical transition lengthscale and provide insights on the transition from inhomogeneous to homogeneous mixing. Note that these models often apply a Lagrangian cloud model in which each computational particle represents one cloud droplet.

DNS models with a coarser resolution and commensurately larger molecular viscosity have also been applied to study small-scale mixing processes in increasingly larger model domains, which enabled deeper insights into inhomogeneous mixing regimes than possible with regular DNS [*Dimotakis*, 2000; *Mellado et al.*, 2010; *de Lozar and Muessle*, 2016; *Mellado et al.*, 2018; *Thomas et al.*, 2020]. However, this approach is limited. The upscaled molecular viscosity might be unable to represent the more complex effects of unresolved turbulent motions at smaller scales adequately, making parameterizations inevitable as further outlined in Sec. 4.2.3 below.

An alternative to DNS are one-dimensional models of turbulence and molecular diffusion [*Kerstein*, 1988; *Jensen and Baker*, 1989; *Krueger et al.*, 1997; *Su et al.*, 1998]. These models are able to resolve the Kolmogorov lengthscale and — due to their reduced dimensionality — can host a model domain of hundreds of meters, even on a simple workstation computer. Of course, turbulence, which naturally requires three dimensions, cannot be represented in these approaches explicitly. However, its effects of compression and folding can be successfully emulated by rearranging or reshaping the model's numerical grid. The specific approach of *Linear Eddy Modeling* (LEM) has been shown to produce results comparable to DNS of the mixing process in clouds [*Krueger*, 2016].

4.2.3 Parameterizations of Turbulent Mixing

To capture entire clouds and the underlying dynamics that drive entrainment and mixing, today's method of choice are *Large Eddy Simulations* (LESs), which solve the filtered Navier-Stokes equations [e.g., *Sagaut*, 2006]. LESs can represent entire cumulus or stratocumulus fields with a horizontal extent of several tens of kilometers successfully [*Siebesma et al.*, 2003; *Stevens et al.*, 2005; *Ackerman et al.*, 2009; *vanZanten et al.*, 2011]. The representation of small-scale processes, however, is limited by their resolution of typically 10 to 100 m. The impact of turbulent mixing on scales below the resolution is usually modeled by a subgrid-scale (SGS) scheme [e.g., *Deardorff*, 1980], which represents the unresolved fluxes of momentum, temperature, and water vapor mixing ratio. By design, the effect of unresolved turbulent mixing on cloud microphysics is homogeneous, which corresponds to the notion that resolved LES quantities represent a grid-box average [*Schumann*, 1975]. Introducing a more realistic representation of SGS mixing is therefore necessary to consider the microphysical effects of small-scale mixing in large-scale models.

Morrison and Grabowski [2008] introduced an approach that can be used with two-moment bulk microphysical models to consider different mixing scenarios. In this approach, the order in which SGS turbulent mixing and evaporation occur in the model is used to adjust the droplet number concentration according to the intended mixing scenario:

$$N = N^* \left(\frac{q_l}{q_l^*} \right)^{\alpha} . \tag{18}$$

Here, N and q_l represent the *final* droplet number concentration and the liquid water content after SGS mixing and evaporation, respectively, while N^* and q_l^* are the corresponding *intermediate* values after SGS mixing but before evaporation. As in Sec. 3.2, α represents the mixing scenario with values between 0 for homogeneous mixing and 1 for extreme inhomogeneous mixing. (It can be shown that (18) is equivalent to (16).) While *Morrison and Grabowski* [2008] prescribe fixed values for α, *Jarecka et al.* [2009, 2013] suggest an approach to predict α based on the Damköhler number. Note that although the parameterization (18) is relatively easy to implement, it is not frequently used in LES or other large-scale models.

Lagrangian cloud models offer simpler ways to include SGS processes than (Eulerian) bulk or bin schemes by making use of the individually simulated computational particles [e.g., *Grabowski et al.*, 2019]. Probably the first approach has been developed by *Grabowski and Abade* [2017], who assumed that each computational particle is surrounded by a volume of air. They used a stochastic Wiener process to model unresolved turbulent supersaturation fluctuations in theses volumes, and considered them in the diffusional growth process of the simulated droplets. Similarly, *Hoffmann et al.* [2019] used the aforementioned one-dimensional LEM by *Kerstein* [1988] to represent unresolved turbulent mixing and molecular diffusion among the volumes of air surrounding each computational particle. Accordingly, this approach enables a very detailed representation of cloudy filaments on scales as small as the transition lengthscale, when used as a SGS model in typical LES applications with Lagrangian cloud microphysics, as recently applied in simulations of cumulus [*Hoffmann et al.*, 2019] and stratocumulus [*Hoffmann and Feingold*, 2019].

5 Effects of Small-Scale Mixing

Observations and numerical modeling enable us to understand the effects of small-scale mixing in frameworks that exceed the simple theoretical considerations presented in Sec. 3. These results will be summarized in this section, dividing them into microscale impacts, which predominantly affect the droplet size distribution and its broadening, and macroscale impacts, which are relevant to the role of clouds in the climate system.

5.1 Microscale Impacts

The basic effects of small-scale mixing on the droplet size distribution have been outlined in Sec. 3: Homogeneous mixing maintains the droplet number and reduces the mean droplet size due to partial evaporation. Extreme inhomogeneous mixing, on the other hand, maintains the mean droplet size, but reduces the droplet number due to the complete evaporation of droplets that leave the cloudy filaments.

An (intermediate) inhomogeneous mixing scenario, however, allows for a large variability in droplet growth histories, including repeated switches between saturated and subsaturated filaments during the mixing process, which leads to a substantial broadening toward smaller droplet sizes by evaporation, as pointed out in numerical studies by *Su et al.* [1998] and *Tölle and Krueger* [2014]. In fact, the broadening to smaller sizes due to entrainment and mixing has been shown essential for initiating the precipitation process in shallow cumulus clouds [*Hoffmann et al.*, 2017]. However, the droplet size distribution does not only experience broadening to smaller sizes. Entrainment generally reduces the droplet concentration in clouds by dilution, irrespective of the mixing scenario (cf. Eqn. (10)). Accordingly, the competition for water vapor is reduced and the droplet size distribution might broaden to larger radii by accelerating the diffusional growth of the remaining droplets if the considered air parcel is still being lifted [e.g., *Lasher-Trapp et al.*, 2005]. This superadiabatic growth can be enhanced in (intermediate or extreme) inhomogeneous mixing scenarios due to the even lower droplet number concentration, as initially hypothesized by *Baker and Latham* [1979] and *Baker et al.* [1980]. Detailed modeling studies confirmed that these superadiabatic droplets can reach sizes that may initiate the precipitation process in warm clouds [*Su et al.*, 1998; *Lasher-Trapp et al.*, 2005; *Tölle and Krueger*, 2014; *Hoffmann et al.*, 2019; *Hoffmann and Feingold*, 2019].

The activation of aerosols to cloud droplets above the cloud base, so-called secondary activation, is frequently observed in cumulus clouds. It is either caused by a substantial increase in the vertical velocity [*Warner*, 1969b; *Pinsky and Khain*, 2002], or by the activation of newly entrained aerosols [*Warner*, 1969a; *Paluch and Knight*, 1984; *Brenguier and Grabowski*, 1993; *Su et al.*, 1998; *Lasher-Trapp et al.*, 2005]. The latter pathway, which dominates in shallow cumulus clouds [*Hoffmann et al.*, 2015; *Chandrakar et al.*, 2021], can be affected by the degree of turbulent mixing. Under rapid mixing, the newly entrained

aerosols compete directly with the (old) cloud droplets for the available water vapor. Since the (old) cloud droplets absorb the water vapor more efficiently due to their larger surface area, the activation of newly entrained aerosols can be reduced. If the mixing is slower, the newly entrained aerosols may be spatially separated from the (old) cloud droplets, which enables a larger fraction of the entrained aerosols to activate [*Su et al.*, 1998; *Lasher-Trapp et al.*, 2005]. While this process broadens the droplet size distribution to smaller radii, it also buffers the negative impact of inhomogeneous mixing on the number of cloud droplets by activating new droplets [*Slawinska et al.*, 2012], complicating the differentiation of homogeneous and inhomogeneous mixing scenarios, as already outlined in Sec. 3.2.

Finally, it is important to reiterate that the mixing character can change with time [e.g., *Jarecka et al.*, 2013]. During a single entrainment event, an initially inhomogeneous mixing scenario can become homogeneous when the entrained air breaks up into filaments with lengthscales below the transition lengthscale (cf. Sec. 3). However, the character of mixing also changes during the cloud lifecycle. *Schmeissner et al.* [2015] derived mixing diagrams from the observation of hundreds of cumulus clouds, showing that actively growing clouds exhibit a more homogeneous mixing character, while clouds in their decaying stage mix more inhomogeneously. *Schmeissner et al.* [2015] explain this behavior by a humid, almost saturated shell that develops during the cumulus lifecycle that prevents the evaporation of cloud droplets in matured cumulus [e.g., *Heus and Jonker*, 2008]. As explained in Sec. 3.2, the high humidity of this shell could also favor a degenerate mixing scenario, in which the microphysical reaction to homogeneous and inhomogeneous mixing is almost indistinguishable [*Korolev et al.*, 2016; *Pinsky et al.*, 2016]. *Schmeissner et al.* [2015], however, interpret the humid shell as part of the inhomogeneous mixing process.

This motivates a fundamental question: What are the largest scales to be included in the small-scale mixing process? The actual entrainment process is happening on the scale of the interfacial eddies of cumulus [*Grabowski and Clark*, 1991] or the holes within a stratocumulus deck [*Nicholls*, 1989]. However, the entrained air on these scales originates from larger scales, namely the humid shells surrounding cumulus [*Heus and Jonker*, 2008] or the entrainment interface layer on top of stratocumulus [*Caughey et al.*, 1982; *Gerber et al.*, 2005; *Yamaguchi and Randall*, 2012]. The thermodynamic composition of these regions is dominated by detrained cloudy filaments evaporating and humidifying these areas in the direct vicinity of the cloud, further modified by radiative cooling or heating [e.g., *Klinger et al.*, 2019]. Additionally, the isotropic turbulence driving small-scale mixing can be superimposed by larger-scale cloud dynamics (e.g., shear instabilities or waves), further changing how the cloud interacts with its environment [e.g., *Mellado*, 2017]. Accordingly, to advance our understanding of small-scale mixing, we need to proceed toward larger scales, requiring us to include processes that have been traditionally neglected.

5.2 Macroscale Impacts

Our understanding of small-scale mixing on the microscale allows us to deduce impacts on the macroscale. As indicated in the introduction, the radiative forcing of clouds on the climate can be understood as the product of cloud albedo and cloud fraction [*Betts*, 2007]. The cloud albedo can be approximated as

$$A \approx \frac{\tau}{\tau + \gamma}, \tag{19}$$

where τ is the cloud optical thickness, and $\gamma \approx 13.3$ depends on the degree of forward scattering for overhead sun [e.g., *Glenn et al.*, 2020]. It can be shown that τ is primarily determined by

$$\tau \propto \mathrm{LWP}^{5/6} N^{1/3}, \tag{20}$$

where LWP is the vertically integrated liquid water content, the so-called liquid water path, and N is the droplet number concentration [e.g., *Boers and Mitchell*, 1994].

Since entrainment determines the amount of non-cloudy air that is engulfed into the cloud, it does not change LWP and N directly. The subsequent small-scale mixing, however, reduces the LWP and N by evaporation and dilution (cf. Eqns. (9) and (10)). The mixing scenario may lead to a further reduction in N, subject to an increasing degree of inhomogeneous mixing (cf. Eqn. (14)), while it does not cause direct changes in LWP. Accordingly, we can already conclude that the mixing scenario affects the cloud albedo by changes in the droplet number concentration, similar to the albedo effect [*Twomey*, 1974, 1977].

The effect of different mixing scenarios on the albedo of numerically simulated clouds has been studied by *Chosson et al.* [2007] and *Slawinska et al.* [2008]. They found that the reduction in cloud albedo due to extreme inhomogeneous mixing instead of homogeneous mixing ranges between 2 and 5 percentage points for stratocumulus and between 5 and 6 percentage points for cumulus, respectively. The strongest dependency has been found for very thin clouds, which is expectable since the optical thickness depends much stronger on the liquid water path than on the droplet number concentration, as indicated by the exponents in Eqn. (20). Accordingly, the albedo of deeper clouds is less susceptible to changes in the number concentration and hence different mixing scenarios. Based on theoretical arguments, *Jeffery* [2007] derived a similar dependence of τ on the mixing scenario.

Much more uncertain are the effects of small-scale mixing on cloud lifetime and cover [e.g., *Albrecht*, 1989]. Two pathways are considered for terminating the lifecycle of a cloud: entrainment or precipitation, which are both potentially modified by small-scale mixing.

Following an entrainment event, inhomogeneous mixing allows droplets to stay in cloudy filaments for a certain period of time, while droplets are more rapidly exposed to subsaturations under homogeneous mixing [*Krueger*, 1993]. Additionally, inhomogeneous mixing reduces the droplet number concentration, resulting in a stronger increase of the phase relaxation timescale than by homogeneous mixing alone, which can further delay the evaporation of cloud droplets [*Hoffmann and Feingold*, 2019]. Accordingly, both processes decelerate the production of negative buoyancy, which is an important driver for the production of turbulence. Thus, the mixing might slow down even further, which could make the mixing process more inhomogeneous. This positive feedback is analogous to the evaporation-entrainment feedback, in which the faster evaporation of a larger number of cloud droplets is suggested to result in stronger turbulence compared to the same amount of water distributed on a smaller number of droplets [*Wang et al.*, 2003; *Xue and Feingold*, 2006; *Glassmeier et al.*, 2021]. The aforementioned authors even showed that this feedback results in increased entrainment rates in droplet-laden conditions, with a commensurately negative impact on the cloud albedo. Nonetheless, entrainment is driven by large-scale cloud dynamics, as outlined in Sec. 2, and a direct impact of small-scale mixing processes must be commensurately weak. Yet, *Hoffmann and Feingold* [2019] showed slightly lower entrainment rates in stratocumulus LES with SGS inhomogeneous mixing compared to simulations with homogeneous SGS mixing.

A more complex situation arises when droplet sedimentation is considered. As already outlined in Sec. 3.1, sedimentation smears out the thermodynamic conditions experienced by a droplet and therefore results in an effectively more rapid mixing scenario [*Tölle and Krueger*, 2014]. Furthermore, sedimentation might also increase the evaporative cooling on the edges of cloudy filaments by exposing droplets to subsaturated air more quickly, as indicated in idealized simulations of *Grabowski* [1993]. As discussed in the last paragraph, a large impact of these small-scale processes on the entrainment rate and hence cloud albedo is unlikely. In fact, LES of stratocumulus (without a special treatment of SGS mixing) indicate generally smaller entrainment rates when sedimentation is considered [*Ackerman et al.*, 2004; *Bretherton et al.*, 2007], which has been confirmed in DNS later [*de Lozar and Mellado*, 2017; *Schulz and Mellado*, 2019]. This process has been explained by the removal of large droplets from the stratocumulus cloud top by sedimentation, which reduces the potential for evaporative cooling in the entrainment interface layer, with a commensurate effect on the evaporative enhancement of the entrainment rate [*Bretherton et al.*, 2007].

By contributing to the initiation of the precipitation process in warm clouds [*Baker and Latham*, 1979; *Lasher-Trapp et al.*, 2005; *Hoffmann et al.*, 2019], inhomogeneous mixing may reduce the lifetime of individual clouds and hence affect cloud cover. However, we do not know yet how entire cloud fields are affected. For instance, enhanced precipitation will contribute to the generation of cold pools, which alter the large-scale organization of cloud fields, with commensurate changes in cloud cover [*Seifert and Heus*, 2013; *Zuidema et al.*, 2017]. Accordingly, there are no conclusive answers on how small-scale mixing affects macroscale cloud properties, especially cloud lifetime and cloud cover. We need more studies that investigate the effects of small-scale mixing on entire cloud fields. Using parameterizations (Sec. 4.2.3) and improving them with detailed modeling (Sec. 4.2.2) seems to be a viable approach.

6 Conclusions

This chapter has been dedicated to our current understanding of the small-scale mixing of clouds with their environment. Although small-scale mixing takes place on scales as small as the Kolmogorov lengthscale, it has fundamental implications for the microphysical composition of clouds and hence their role in the climate system, most significantly by altering the ability of clouds to reflect incident shortwave radiation back to space.

For more than 50 years, small-scale mixing has been investigated in numerous studies employing theory, observations, and numerical modeling. However, our understanding of small-scale mixing is not complete. Limitations primarily consider the interaction of large and small scales. While increasing computational power will solve some problems, especially when larger scales are approached from below, the growing importance of processes that have been traditionally neglected in the discussion of small-scale mixing, e.g., radiation and larger-scale cloud dynamics, demand careful consideration in the future. Our understanding of small-scale mixing on global scales, however, will still depend on parameterizations in the next decades. Accordingly, developing successful parameterizations of small-scale mixing will be essential to assess the role of small-scale mixing in the climate system. New insights are also expected from the development of new observational approaches such as remotely operated aircrafts (i.e., drones), as well as larger laboratory facilities in which a much wider range of scales relevant to the mixing process can be analyzed.

All in all, small-scale mixing in clouds offers ample opportunities for future research from a large variety of backgrounds and with potentially large impacts on our understanding of clouds in the climate system.

Acknowledgments

This chapter benefitted from discussions with Graham Feingold, and comments by Wojciech Grabowski, Steven Krueger, and one anonymous referee. The author acknowledges support from the Emmy Noether program of the German Research Foundation (DFG) under grant HO 6588/1-1.

References

Abade, G. C., W. W. Grabowski, and H. Pawlowska (2018), Broadening of cloud droplet spectra through eddy hopping: Turbulent entraining parcel simulations, *J. Atmos. Sci.*, *75*(10), 3365–3379.

Ackerman, A. S., M. P. Kirkpatrick, D. E. Stevens, and O. B. Toon (2004), The impact of humidity above stratiform clouds on indirect aerosol climate forcing, *Nature*, *432*(7020), 1014.

Ackerman, A. S., M. C. VanZanten, B. Stevens, V. Savic-Jovcic, C. S. Bretherton, A. Chlond, J.-C. Golaz, H. Jiang, M. Khairoutdinov, S. K. Krueger, et al. (2009), Large-eddy simulations of a drizzling, stratocumulus-topped marine boundary layer., *Mon. Wea. Rev.*,

137(3).

Albrecht, B. A. (1989), Aerosols, cloud microphysics, and fractional cloudiness, *Science*, *245*(4923), 1227–1230.

Andrejczuk, M., J. M. Reisner, B. Henson, M. K. Dubey, and C. A. Jeffery (2008), The potential impacts of pollution on a nondrizzling stratus deck: Does aerosol number matter more than type?, *J. Geophys. Res.*, *113*(D19204).

Andrejczuk, M., W. W. Grabowski, S. P. Malinowski, and P. K. Smolarkiewicz (2009), Numerical simulation of cloud–clear air interfacial mixing: Homogeneous versus inhomogeneous mixing, *J. Atmos. Sci.*, *66*(8), 2493–2500.

Arabas, S., and S.-i. Shima (2017), On the ccn (de) activation nonlinearities, *Nonlinear Process. Geophys.*, *24*(3), 535–542.

Baker, M., and J. Latham (1979), The evolution of droplet spectra and the rate of production of embryonic raindrops in small cumulus clouds, *J. Atmos. Sci.*, *36*(8), 1612–1615.

Baker, M., R. Corbin, and J. Latham (1980), The influence of entrainment on the evolution of cloud droplet spectra: I. a model of inhomogeneous mixing, *Quart. J. Roy. Meteor. Soc.*, *106*(449), 581–598.

Baker, M. B., R. E. Breidenthal, T. W. Choularton, and J. Latham (1984), The effects of turbulent mixing in clouds., *J. Atmos. Sci.*, *41*, 299–304.

Beals, M. J., J. P. Fugal, R. A. Shaw, J. Lu, S. M. Spuler, and J. L. Stith (2015), Holographic measurements of inhomogeneous cloud mixing at the centimeter scale, *Science*, *350*(6256), 87–90.

Betts, A. K. (2007), Coupling of water vapor convergence, clouds, precipitation, and land-surface processes, *J. Geophys. Res.*, *112*(D10).

Blyth, A. M., W. A. Cooper, and J. B. Jensen (1988), A study of the source of entrained air in montana cumuli, *J. Atmos. Sci.*, *45*, 3944–3964.

Bodenschatz, E., S. P. Malinowski, R. A. Shaw, and F. Stratmann (2010), Can we understand clouds without turbulence?, *Science*, *327*(5968), 970–971.

Boers, R., and R. M. Mitchell (1994), Absorption feedback in stratocumulus clouds influence on cloud top albedo, *Tellus A*, *46*(3), 229–241.

Bott, A. (1998), A flux method for the numerical solution of the stochastic collection equation, *J. Atmos. Sci.*, *55*(13), 2284–2293.

Boucher, O., D. Randall, P. Artaxo, C. Bretherton, G. Feingold, P. Forster, V.-M. Kerminen, Y. Kondo, H. Liao, U. Lohmann, et al. (2013), Clouds and aerosols, in *Climate change 2013: the physical science basis. Contribution of Working Group I to the Fifth Assessment Report of the Intergovernmental Panel on Climate Change*, pp. 571–657, Cambridge University Press.

Brenguier, J.-L. (1993), Observations of cloud microstructure at the centimeter scale, *J. Appl. Meteor. Climatol.*, *32*(4), 783–793.

Brenguier, J.-L., and W. W. Grabowski (1993), Cumulus entrainment and cloud droplet spectra: A numerical model within a two-dimensional dynamical framework, *J. Atmos. Sci.*, *50*(1), 120 – 136, doi:10.1175/1520-0469(1993)050<0120:CEACDS>2.0.CO;2.

Brenguier, J.-L., T. Bourrianne, A. A. Coelho, J. Isbert, R. Peytavi, D. Trevarin, and P. Weschler (1998), Improvements of droplet size distribution measurements with the fast-fssp (forward scattering spectrometer probe), *J. Atmos. Oceanic Technol.*, *15*(5), 1077–1090.

Bretherton, C., P. N. Blossey, and J. Uchida (2007), Cloud droplet sedimentation, entrainment efficiency, and subtropical stratocumulus albedo, *Geophys. Res. Lett.*, *34*(3).

Burnet, F., and J.-L. Brenguier (2007), Observational study of the entrainment-mixing process in warm convective clouds, *J. Atmos. Sci.*, *64*(6), 1995–2011.

Caughey, S., B. Crease, and W. Roach (1982), A field study of nocturnal stratocumulus ii turbulence structure and entrainment, *Quart. J. Roy. Meteor. Soc.*, *108*(455), 125–144.

Chandrakar, K. K., W. W. Grabowski, H. Morrison, and G. H. Bryan (2021), Impact of entrainment-mixing and turbulent fluctuations on droplet size distributions in a cumulus cloud: An investigation using lagrangian microphysics with a sub-grid-scale model, *J. At-*

mos. Sci., *under review*.

Chang, K., J. Bench, M. Brege, W. Cantrell, K. Chandrakar, D. Ciochetto, C. Mazzoleni, L. Mazzoleni, D. Niedermeier, and R. Shaw (2016), A laboratory facility to study gas–aerosol–cloud interactions in a turbulent environment: The π chamber, *Bull. Amer. Meteor. Soc.*, *97*(12), 2343–2358.

Chosson, F., J.-L. Brenguier, and L. Schüller (2007), Entrainment-mixing and radiative transfer simulation in boundary layer clouds, *J. Atmos. Sci.*, *64*(7), 2670–2682.

Cooper, W. A. (1989), Effects of variable droplet growth histories on droplet size distributions. part i: Theory, *J. Atmos. Sci.*, *46*(10), 1301–1311.

de Lozar, A., and J. P. Mellado (2017), Reduction of the entrainment velocity by cloud droplet sedimentation in stratocumulus, *J. Atmos. Sci.*, *74*(3), 751–765.

de Lozar, A., and L. Muessle (2016), Long-resident droplets at the stratocumulus top, *Atmos. Chem. Phys.*, *16*(10), 6563–6576.

de Rooy, W. C., P. Bechtold, K. Fröhlich, C. Hohenegger, H. Jonker, D. Mironov, A. P. Siebesma, J. Teixeira, and J.-I. Yano (2013), Entrainment and detrainment in cumulus convection: an overview, *Quart. J. Roy. Meteor. Soc.*, *139*(670), 1–19, doi:10.1002/qj.1959.

Deardorff, J. W. (1980), Stratocumulus-capped mixed layers derived from a three-dimensional model, *Boundary-Layer Meteor.*, *18*(4), 495–527.

Devenish, B., P. Bartello, J.-L. Brenguier, L. Collins, W. Grabowski, R. IJzermans, S. Malinowski, M. Reeks, J. Vassilicos, L.-P. Wang, et al. (2012), Droplet growth in warm turbulent clouds, *Quart. J. Roy. Meteor. Soc.*, *138*(667), 1401–1429.

Dimotakis, P. E. (2000), The mixing transition in turbulent flows, *J. Fluid Mech.*, *409*, 69–98.

Feingold, G., and H. Siebert (2009), Cloud-aerosol interactions from the micro to the cloud scale, in *Clouds in the perturbed climate system: their relationship to energy balance, atmospheric dynamics, and precipitation, Strüngmann Forum Report,*, edited by J. Heintzenberg and R. Charlson, The MIT Press.

Gao, Z., Y. Liu, X. Li, and C. Lu (2018), Investigation of turbulent entrainment-mixing processes with a new particle-resolved direct numerical simulation model, *J. Geophys. Res.*, *123*(4), 2194–2214.

Gerber, H., B. G. Arends, and A. S. Ackerman (1993), New microphysics sensor for aircraft use, *Atmos. Res.*, *31*, 235–252, doi:10.1016/0169-8095(94)90001-9.

Gerber, H., G. Frick, S. Malinowski, J. Brenguier, and F. Burnet (2005), Holes and entrainment in stratocumulus, *J. Atmos. Sci.*, *62*(2), 443–459.

Gerber, H. E., G. M. Frick, J. B. Jensen, and J. G. Hudson (2008), Entrainment, mixing, and microphysics in trade-wind cumulus, *J. Meteor. Soc. Japan*, *86*, 87–106.

Glassmeier, F., F. Hoffmann, J. S. Johnson, T. Yamaguchi, K. S. Carslaw, and G. Feingold (2021), Aerosol-cloud-climate cooling overestimated by ship-track data, *Science*, *371*(6528), 485–489.

Glenn, I. B., G. Feingold, J. J. Gristey, and T. Yamaguchi (2020), Quantification of the radiative effect of aerosol–cloud interactions in shallow continental cumulus clouds, *J. Atmos. Sci.*, *77*(8), 2905 – 2920, doi:10.1175/JAS-D-19-0269.1.

Götzfried, P., B. Kumar, R. A. Shaw, and J. Schumacher (2017), Droplet dynamics and fine-scale structure in a shearless turbulent mixing layer with phase changes, *J. Fluid Mech.*, *814*, 452–483.

Grabowski, W. W. (1993), Cumulus entrainment, fine-scale mixing, and buoyancy reversal, *Quart. J. Roy. Meteor. Soc.*, *119*(513), 935–956.

Grabowski, W. W., and G. C. Abade (2017), Broadening of cloud droplet spectra through eddy hopping: Turbulent adiabatic parcel simulations, *J. Atmos. Sci.*, doi:10.1175/JAS-D-17-0043.1.

Grabowski, W. W., and T. L. Clark (1991), Cloud–environment interface instability: Rising thermal calculations in two spatial dimensions, *J. Atmos. Sci.*, *48*(4), 527–546.

Grabowski, W. W., and T. L. Clark (1993), Cloud-environment interface instability: Part ii: Extension to three spatial dimensions, *J. Atmos. Sci.*, *50*(4), 555 – 573, doi:10.1175/1520-

0469(1993)050<0555:CEIIPI>2.0.CO;2.

Grabowski, W. W., and P. Vaillancourt (1999), Comments on "preferential concentration of cloud droplets by turbulence: effects on the early evolution of cumulus cloud droplet spectra", *J. Atmos. Sci.*, *56*(10), 1433–1436.

Grabowski, W. W., and L.-P. Wang (2013), Growth of cloud droplets in a turbulent environment, *Annu. Rev. Fluid Mech.*, *45*, 293–324.

Grabowski, W. W., H. Morrison, S.-I. Shima, G. C. Abade, P. Dziekan, and H. Pawlowska (2019), Modeling of cloud microphysics: Can we do better?, *Bull. Amer. Meteor. Soc.*, *100*(4), 655 – 672, doi:10.1175/BAMS-D-18-0005.1.

Heus, T., and H. J. J. Jonker (2008), Subsiding shells around shallow cumulus clouds, *J. Atmos. Sci.*, *65*(3), 1003–1018.

Heus, T., G. Van Dijk, H. J. Jonker, and H. E. Van den Akker (2008), Mixing in shallow cumulus clouds studied by lagrangian particle tracking, *J. Atmos. Sci.*, *65*(8), 2581–2597.

Hoffmann, F. (2020), Effects of entrainment and mixing on the wegener–bergeron–findeisen process, *J. Atmos. Sci.*, *77*(6), 2279–2296.

Hoffmann, F., and G. Feingold (2019), Entrainment and mixing in stratocumulus: Effects of a new explicit subgrid-scale scheme for large-eddy simulations with particle-based microphysics, *J. Atmos. Sci.*, *76*(7), 1955–1973.

Hoffmann, F., S. Raasch, and Y. Noh (2015), Entrainment of aerosols and their activation in a shallow cumulus cloud studied with a coupled LCM-LES approach, *Atmos. Res.*, *156*, 43–57.

Hoffmann, F., Y. Noh, and S. Raasch (2017), The route to raindrop formation in a shallow cumulus cloud simulated by a lagrangian cloud model, *J. Atmos. Sci.*, *74*(7), 2125–2142.

Hoffmann, F., T. Yamaguchi, and G. Feingold (2019), Inhomogeneous mixing in lagrangian cloud models: Effects on the production of precipitation embryos, *J. Atmos. Sci.*, *76*(1), 113–133, doi:10.1175/JAS-D-18-0087.1.

Jarecka, D., W. W. Grabowski, and H. Pawlowska (2009), Modeling of subgrid-scale mixing in large-eddy simulation of shallow convection, *J. Atmos. Sci.*, *66*(7), 2125–2133, doi:10.1175/2009JAS2929.1.

Jarecka, D., W. W. Grabowski, H. Morrison, and H. Pawlowska (2013), Homogeneity of the subgrid-scale turbulent mixing in large-eddy simulation of shallow convection, *J. Atmos. Sci.*, *70*(9), 2751–2767.

Jeffery, C. A. (2007), Inhomogeneous cloud evaporation, invariance, and damköhler number, *J. Geophys. Res.*, *112*(D24).

Jensen, J., P. Austin, M. Baker, and A. Blyth (1985), Turbulent mixing, spectral evolution and dynamics in a warm cumulus cloud, *J. Atmos. Sci.*, *42*(2), 173–192.

Jensen, J. B., and M. B. Baker (1989), A simple model of droplet spectral evolution during turbulent mixing, *J. Atmos. Sci.*, *46*(18), 2812–2829.

Kerstein, A. R. (1988), A linear-eddy model of turbulent scalar transport and mixing, *Combust. Sci. Technol.*, *60*(4-6), 391–421.

Khairoutdinov, M., and Y. Kogan (2000), A new cloud physics parameterization in a large-eddy simulation model of marine stratocumulus, *Mon. Wea. Rev.*, *128*(1), 229–243.

Klinger, C., G. Feingold, and T. Yamaguchi (2019), Cloud droplet growth in shallow cumulus clouds considering 1-d and 3-d thermal radiative effects., *Atmos. Chem. Phys.*, *19*(9).

Korolev, A., A. Khain, M. Pinsky, and J. French (2016), Theoretical study of mixing in liquid clouds–part 1: Classical concepts, *Atmos. Chem. Phys.*, *16*(14).

Korolev, A., G. McFarquhar, P. R. Field, C. Franklin, P. Lawson, Z. Wang, E. Williams, S. J. Abel, D. Axisa, S. Borrmann, et al. (2017), Mixed-phase clouds: Progress and challenges, *Meteorol. Monogr.*, *58*, 5–1.

Krueger, S. K. (1993), Linear eddy modeling of entrainment and mixing in stratus clouds, *J. Atmos. Sci.*, *50*(18), 3078–3090.

Krueger, S. K. (2016), Representing the effects of entrainment and mixing on warm-cloud microphysics in large-eddy simulations, in *AGU Fall Meeting Abstracts*.

826 Krueger, S. K., C.-W. Su, and P. A. McMurtry (1997), Modeling entrainment and finescale
827 mixing in cumulus clouds, *J. Atmos. Sci.*, *54*(23), 2697–2712.
828 Kumar, B., J. Schumacher, and R. A. Shaw (2013), Cloud microphysical effects of turbulent
829 mixing and entrainment, *Theo. Comput. Fluid Dyn.*, *27*(3-4), 361–376.
830 Kunishima, Y., and R. Onishi (2018), Direct lagrangian tracking simulation of droplet
831 growth in vertically developing cloud, *Atmos. Chem. Phys.*, *18*(22), 16,619–16,630, doi:
832 10.5194/acp-18-16619-2018.
833 Kurowski, M. J., S. P. Malinowski, and W. W. Grabowski (2009), A numerical investigation
834 of entrainment and transport within a stratocumulus-topped boundary layer, *Quart. J. Roy.*
835 *Meteor. Soc.*, *135*(638), 77–92, doi:https://doi.org/10.1002/qj.354.
836 Lasher-Trapp, S. G., W. A. Cooper, and A. M. Blyth (2005), Broadening of droplet size dis-
837 tributions from entrainment and mixing in a cumulus cloud, *Quart. J. Roy. Meteor. Soc.*,
838 *131*(605), 195–220.
839 Latham, J., and R. Reed (1977), Laboratory studies of the effects of mixing on the evolution
840 of cloud droplet spectra, *Quart. J. Roy. Meteor. Soc.*, *103*(436), 297–306.
841 Lehmann, K., H. Siebert, and R. A. Shaw (2009), Homogeneous and inhomogeneous mix-
842 ing in cumulus clouds: Dependence on local turbulence structure, *J. Atmos. Sci.*, *66*(12),
843 3641–3659.
844 Lu, C., Y. Liu, S. Niu, S. Krueger, and T. Wagner (2013), Exploring parameterization for
845 turbulent entrainment-mixing processes in clouds, *J. Geophys. Res.*, *118*(1), 185–194.
846 Lu, C., Y. Liu, B. Zhu, S. S. Yum, S. K. Krueger, Y. Qiu, S. Niu, and S. Luo (2018), On
847 which microphysical time scales to use in studies of entrainment-mixing mechanisms in
848 clouds, *J. Geophys. Res.*, *123*(7), 3740–3756.
849 Luo, S., C. Lu, Y. Liu, J. Bian, W. Gao, J. Li, X. Xu, S. Gao, S. Yang, and X. Guo (2020),
850 Parameterizations of entrainment-mixing mechanisms and their effects on cloud droplet
851 spectral width based on numerical simulations, *J. Geophys. Res.*, *accepted*.
852 Maury, N., G. C. Roberts, F. Couvreux, T. Verdu, P. Narvor, N. Villefranque, S. Lacroix, and
853 G. Hattenberger (2021), Use of large-eddy simulations to design an adaptive sampling
854 strategy to assess cumulus cloud heterogeneities by remotely piloted aircraft, *Atmos. Meas.*
855 *Tech. Discuss.*, *2021*, 1–26, doi:10.5194/amt-2021-20.
856 Mellado, J. P. (2017), Cloud-top entrainment in stratocumulus clouds, *Annu. Rev. Fluid*
857 *Mech.*, *49*, 145–169.
858 Mellado, J. P., B. Stevens, H. Schmidt, and N. Peters (2010), Two-fluid formulation of the
859 cloud-top mixing layer for direct numerical simulation, *Theo. Comput. Fluid Dyn.*, *24*(6),
860 511–536.
861 Mellado, J.-P., C. Bretherton, B. Stevens, and M. Wyant (2018), Dns and les for simulating
862 stratocumulus: Better together, *J. Adv. Model. Earth Syst.*
863 Milbrandt, J., and M. Yau (2005), A multimoment bulk microphysics parameterization. part
864 i: Analysis of the role of the spectral shape parameter., *J. Atmos. Sci.*, *62*(9).
865 Moin, P., and K. Mahesh (1998), Direct numerical simulation: a tool in turbulence research,
866 *Annu. Rev. Fluid Mech.*, *30*(1), 539–578.
867 Morrison, H., and W. W. Grabowski (2008), Modeling supersaturation and subgrid-scale
868 mixing with two-moment bulk warm microphysics, *J. Atmos. Sci.*, *65*(3), 792–812.
869 Morrison, H., J. Curry, and V. Khvorostyanov (2005), A new double-moment microphysics
870 parameterization for application in cloud and climate models. part i: Description, *J. At-*
871 *mos. Sci.*, *62*(6), 1665–1677.
872 Morrison, H., M. van Lier-Walqui, A. M. Fridlind, W. W. Grabowski, J. Y. Harrington,
873 C. Hoose, A. Korolev, M. R. Kumjian, J. A. Milbrandt, H. Pawlowska, et al. (2020), Con-
874 fronting the challenge of modeling cloud and precipitation microphysics, *J. Adv. Model.*
875 *Earth Syst.*, *12*(8), e2019MS001,689.
876 Nicholls, S. (1989), The structure of radiatively driven convection in stratocumulus, *Quart. J.*
877 *Roy. Meteor. Soc.*, *115*(487), 487–511.
878 Paluch, I. R. (1986), Mixing and the cloud droplet size spectrum: Generalizations from the
879 ccope data, *J. Atmos. Sci.*, *43*(18), 1984–1993.

Paluch, I. R., and D. G. Baumgardner (1989), Entrainment and fine-scale mixing in a continental convective cloud, *J. Atmos. Sci.*, *46*(2), 261–278.

Paluch, I. R., and C. A. Knight (1984), Mixing and the evolution of cloud droplet size spectra in a vigorous continental cumulus, *J. Atmos. Sci.*, *41*(11), 1801 – 1815, doi:10.1175/1520-0469(1984)041<1801:MATEOC>2.0.CO;2.

Perrin, V. E., and H. J. J. Jonker (2015), Lagrangian droplet dynamics in the subsiding shell of a cloud using direct numerical simulations, *J. Atmos. Sci.*, *72*(10), 4015 – 4028, doi: 10.1175/JAS-D-15-0045.1.

Peters, N. (2000), *Turbulent Combustion*, Cambridge University Press, Cambridge.

Pinsky, M., and A. Khain (2002), Effects of in-cloud nucleation and turbulence on droplet spectrum formation in cumulus clouds, *Quart. J. Roy. Meteor. Soc.*, *128*(580), 501–533.

Pinsky, M., A. Khain, and A. Korolev (2016), Theoretical analysis of mixing in liquid clouds–part 3: Inhomogeneous mixing, *Atmos. Chem. Phys.*, *16*(14), 9273–9297.

Sagaut, P. (2006), *Large eddy simulation for incompressible flows*, Springer, Berlin.

Schmeissner, T., R. Shaw, J. Ditas, F. Stratmann, M. Wendisch, and H. Siebert (2015), Turbulent mixing in shallow trade wind cumuli: Dependence on cloud life cycle, *J. Atmos. Sci.*, *72*(4), 1447–1465.

Schulz, B., and J. P. Mellado (2019), Competing effects of droplet sedimentation and wind shear on entrainment in stratocumulus, *J. Adv. Model. Earth Syst.*, *11*(6), 1830–1846, doi: https://doi.org/10.1029/2019MS001617.

Schumann, U. (1975), Subgrid scale model for finite difference simulations of turbulent flows in plane channels and annuli, *J. Comput. Phys.*, *18*(4), 376–404.

Seifert, A., and K. D. Beheng (2006), A two-moment cloud microphysics parameterization for mixed-phase clouds. Part 1: Model description, *Meteorol. Atmos. Phys.*, *92*, 45–66.

Seifert, A., and T. Heus (2013), Large-eddy simulation of organized precipitating trade wind cumulus clouds, *Atmos. Chem. Phys.*, *13*.

Shaw, R. A. (2003), Particle-turbulence interactions in atmospheric clouds, *Annu. Rev. Fluid Mech.*, *35*(1), 183–227, doi:10.1146/annurev.fluid.35.101101.161125.

Shaw, R. A., W. Cantrell, S. Chen, P. Chuang, N. Donahue, G. Feingold, P. Kollias, A. Korolev, S. Kreidenweis, S. Krueger, et al. (2020), Cloud–aerosol–turbulence interactions: Science priorities and concepts for a large-scale laboratory facility, *Bull. Amer. Meteor. Soc.*, *101*(7), E1026–E1035.

Shima, S.-I., K. Kusano, A. Kawano, T. Sugiyama, and S. Kawahara (2009), The super-droplet method for the numerical simulation of clouds and precipitation: A particle-based and probabilistic microphysics model coupled with a non-hydrostatic model, *Quart. J. Roy. Meteor. Soc.*, *135*(642), 1307–1320.

Siebert, H., K. Lehmann, and M. Wendisch (2006), Observations of small-scale turbulence and energy dissipation rates in the cloudy boundary layer, *J. Atmos. Sci.*, *63*(5), 1451–1466.

Siebert, H., M. Beals, J. Bethke, E. Bierwirth, T. Conrath, K. Dieckmann, F. Ditas, A. Ehrlich, D. Farrell, S. Hartmann, M. A. Izaguirre, J. Katzwinkel, L. Nuijens, G. Roberts, M. Schäfer, R. A. Shaw, T. Schmeissner, I. Serikov, B. Stevens, F. Stratmann, B. Wehner, M. Wendisch, F. Werner, and H. Wex (2013), The fine-scale structure of the trade wind cumuli over barbados – an introduction to the carriba project, *Atmospheric Chemistry and Physics*, *13*(19), 10,061–10,077, doi:10.5194/acp-13-10061-2013.

Siebesma, A. P., C. S. Bretherton, A. R. Brown, A. Chlond, J. Cuxart, P. G. Duynkerke, H. Jiang, M. Khairoutdinov, D. Lewellen, C.-H. Moeng, E. Sanchez, B. Stevens, and D. E. Stevens (2003), A large eddy simulation intercomparison study of shallow cumulus convection, *J. Atmos. Sci.*, *60*, 1201–1219.

Slawinska, J., W. W. Grabowski, H. Pawlowska, and A. A. Wyszogrodzki (2008), Optical properties of shallow convective clouds diagnosed from a bulk-microphysics large-eddy simulation, *J. Climate*, *21*(7), 1639–1647.

Slawinska, J., W. W. Grabowski, H. Pawlowska, and H. Morrison (2012), Droplet activation and mixing in large-eddy simulation of a shallow cumulus field, *J. Atmos. Sci.*, *69*, 444–

462.

Squires, P. (1952), The growth of cloud drops by condensation. i. general characteristics, *Aust. J. Sci. Res.*, *5*(1), 59–86.

Stevens, B., C.-H. Moeng, A. S. Ackerman, C. S. Bretherton, A. Chlond, S. de Roode, J. Edwards, J.-C. Golaz, H. Jiang, M. Khairoutdinov, et al. (2005), Evaluation of large-eddy simulations via observations of nocturnal marine stratocumulus, *Mon. Wea. Rev.*, *133*(6), 1443–1462.

Stommel, H. (1947), Entrainment of air into a cumulus cloud: (paper presented 27 december 1946 at the annual meeting, ams, cambridge, massachusetts), *J. Meteor.*, *4*(3), 91–94.

Su, C.-W., S. K. Krueger, P. A. McMurtry, and P. H. Austin (1998), Linear eddy modeling of droplet spectral evolution during entrainment and mixing in cumulus clouds, *Atmos. Res.*, *47*, 41–58.

Thomas, L., W. W. Grabowski, and B. Kumar (2020), Diffusional growth of cloud droplets in homogeneous isotropic turbulence: Dns, scaled-up dns, and stochastic model, *Atmos. Chem. Phys.*, *20*(14), 9087–9100.

Thompson, G., and T. Eidhammer (2014), A study of aerosol impacts on clouds and precipitation development in a large winter cyclone, *J. Atmos. Sci.*, *71*(10), 3636–3658.

Tölle, M. H., and S. K. Krueger (2014), Effects of entrainment and mixing on droplet size distributions in warm cumulus clouds, *J. Adv. Model. Earth Syst.*, *6*(2), 281–299.

Twomey, S. (1974), Pollution and the planetary albedo, *Atmos. Environ.*, *8*(12), 1251–1256.

Twomey, S. (1977), The influence of pollution on the shortwave albedo of clouds, *J. Atmos. Sci.*, *34*(7), 1149–1152.

Tzivion, S., G. Feingold, and Z. Levin (1987), An efficient numerical solution to the stochastic collection equation, *J. Atmos. Sci.*, *44*(21), 3139–3149.

Vaillancourt, P., M. Yau, P. Bartello, and W. W. Grabowski (2002), Microscopic approach to cloud droplet growth by condensation. part ii: Turbulence, clustering, and condensational growth, *J. Atmos. Sci.*, *59*(24), 3421–3435.

Vaillancourt, P. A., M. K. Yau, and W. W. Grabowski (2001), Microscopic approach to cloud droplet growth by condensation. part i: Model description and results without turbulence, *J. Atmos. Sci.*, *58*(14), 1945 – 1964, doi:10.1175/1520-0469(2001)058<1945:MATCDG>2.0.CO;2.

vanZanten, M. C., B. Stevens, L. Nuijens, A. P. Siebesma, A. S. Ackerman, F. Burnet, A. Cheng, F. Couvreux, H. Jiang, M. Khairoutdinov, Y. Kogan, D. C. Lewellen, D. Mechem, K. Nakamura, A. Noda, B. J. Shipway, J. Slawinska, S. Wang, and A. Wyszogrodzki (2011), Controls on precipitation and cloudiness in simulations of trade-wind cumulus as observed during rico, *J. Adv. Model. Earth Syst.*, *3*(2), doi:10.1029/2011MS000056.

Wang, S., Q. Wang, and G. Feingold (2003), Turbulence, condensation, and liquid water transport in numerically simulated nonprecipitating stratocumulus clouds, *J. Atmos. Sci.*, *60*(2), 262–278.

Warner, J. (1955), The water content of cumuliform cloud, *Tellus*, *7*(4), 449–457, doi:https://doi.org/10.1111/j.2153-3490.1955.tb01183.x.

Warner, J. (1969a), The microstructure of cumulus cloud. part i. general features of the droplet spectrum, *J. Atmos. Sci.*, *26*(5), 1049 – 1059, doi:10.1175/1520-0469(1969)026<1049:TMOCCP>2.0.CO;2.

Warner, J. (1969b), The microstructure of cumulus cloud. part ii. the effect on droplet size distribution of the cloud nucleus spectrum and updraft velocity, *J. Atmos. Sci.*, *26*(6), 1272 – 1282, doi:10.1175/1520-0469(1969)026<1272:TMOCCP>2.0.CO;2.

Warner, J. (1973), The microstructure of cumulus cloud. part iv. the effect on the droplet spectrum of mixing between cloud and environment, *J. Atmos. Sci.*, *30*(2), 256–261.

Xue, H., and G. Feingold (2006), Large-eddy simulations of trade wind cumuli: Investigation of aerosol indirect effects, *J. Atmos. Sci.*, *63*(6), 1605–1622.

Yamaguchi, T., and D. A. Randall (2012), Cooling of entrained parcels in a large-eddy simulation, *J. Atmos. Sci.*, *69*(3), 1118–1136.

Zhao, M., and P. H. Austin (2005), Life cycle of numerically simulated shallow cumulus clouds. Part II: Mixing dynamics, *J. Atmos. Sci.*, *62*, 1291–1310.

Zuidema, P., G. Torri, C. Muller, and A. Chandra (2017), A survey of precipitation-induced atmospheric cold pools over oceans and their interactions with the larger-scale environment, *Surv. Geophys.*, *38*(6), 1283–1305.